Progress In Electromagnetics Research M, Vol. 113, 151–161, 2022

Dual-Band Nanostructured Polarizer

Ragib S. Rafi* **and Alessandro Salandrino**

Abstract—We propose the design of a dual-band nano-structured polarizer that allows the transmission of two different linear polarizations within different frequency bands. A broad-band transmission window in the visible range exists for the x-polarization, whereas the y-polarization transmits efficiently in the near-infrared range. The transmittance exceeds 80% for the target polarization in both cases under normal incidence. This operation is achieved by an orthogonally patterned metallic surface having a long metal wire along the x-axis with four other small metal wires along the y-axis and allowing for a strong localized slit resonance to operate in the desired passband. The appropriate metal length and air gap choice lead to intense slit resonances in the spectral region of choice. The proposed design can be optimized for either ultrawide single band operation or dual-band perpendicular polarization operation.

1. INTRODUCTION

Polarization control plays an important role in optical devices and systems. The design of the polarizer is crucial to how efficiently polarization can be controlled [1–3]. Polarizers should be designed for compatibility with the goal of miniaturization and integration for modern optical systems and be suitable for varied applications such as displays, imaging, beam shaping, sensing, optical measurements, and medical applications, to name a few. Increasing opportunities and possible applications in the visible and infrared frequency ranges offer open research challenges to design and fabricate novel optical devices in those regions [4–6]. However, significant limitations for designing these exotic optical components are imposed by circumstances such as limits to fabrication and device integration, the bulky nature of existing optical devices, and the lack of suitable permittivity and permeability-based natural materials. These obstacles have directed some research towards artificial materials based on different applications. Additionally, features like strong light-matter interaction and wavefront shaping capability make artificial nanostructures-based planar materials suitable for polarization optics [7, 8]. The inclusion of metals allows for applications like plasmonic polarizers, resonators, and sensors.

Plasmonic polarizer designs mostly employ periodic arrangements of subwavelength metallic wire grids on top of a substrate. These designs vary wire grid length, width, depth, and periodicity to maximize transmission efficiency for the desired polarization in the operating frequency bands while minimizing that of the other polarization. Several other approaches based on monolayer, bilayer, or multilayer structures are being investigated, along with varying metal wire shapes and sizes. These include using different metals (Au, Ag, Cu, Al, Cr, etc.) for wires in addition to complex nanoantenna and nanoparticle-based designs [9–16]. Much of the recently published research on achieving multifunctional artificial structures in different frequency bands based on different polarizations consists of multilayered structures with complex designs and composite materials such as vanadium dioxide, indium tin oxide, hafnium oxide, and others [17–20]. Such results show mostly broad range reflection-based performance or efficient diffraction efficiency ($> 65\%$) in a narrow band (100–150 nm bandwidth range) [17, 20]. Therefore, the search for high transmittance-based broadband

---

Received 31 July 2022, Accepted 9 September 2022, Scheduled 19 September 2022

* Corresponding author: Ragib Shakil Rafi (ragib@ku.edu).
The authors are with the Electrical Engineering and Computer Science, University of Kansas, Lawrence, KS 66045, USA.

plasmonic polarizer design for different polarizations remains ongoing. A polarizer that can perform differently in different bands, such as visible and near-infrared, based on incident polarization would be an exotic optical device since controlling the high negative permittivity of metals in the near-infrared and, especially, visible regions is a tricky objective. Physical phenomena such as the excitation of surface plasmon resonances, as well as design choices aimed at controlling the anisotropy of nanostructures, creating a waveguiding mechanism for the desired polarization, and reducing the impedance mismatch between metal and substrate to initiate Fabry-Perot resonance are behind the working principles of plasmonic polarizers [21–23]. A technical challenge is creating a compact device that enables these phenomena in different bands over a broad wavelength range with minimum loss.

We propose a metallic wire-based plasmonic polarizer that allows one linear polarization state with the electric field oriented in the x-axis direction (henceforth denoted as "x-polarization") to pass in the visible range while canceling it in the infrared region, whereas the orthogonal linear polarization state-oriented in the y-axis direction ("y-polarization") is suppressed in the visible region and efficiently transmitted in the near-infrared range. Our proposed structure comprises a 400 nm-thick layer of metallic gold above a silicon substrate which provides $> 80\%$ transmission efficiency for the x-and y-polarization in the 550–850 nm and 1300–1800 nm wavelength ranges, respectively. The impact of the metal thickness, width, air gaps between metal wires, and periodicity are investigated and discussed in detail to elucidate the working principles of the proposed design. Finally, two metrics: the degree of polarization and polarization extinction ratio, are calculated over the entire working bandwidth of the polarizer.

The paper's organization follows the introduction of the rigorous coupled wave analysis (RCWA) method for our simulation, the description of the proposed structures and materials, and finally results and discussion.

2. NUMERICAL SIMULATION METHOD AND MODEL

2.1. Simulation Method

To analyze the proposed model, we used our own implementation of the rigorous coupled wave analysis (RCWA) method in MATLAB. RCWA is a semi-analytical Fourier space method first introduced to describe the diffraction of electromagnetic waves by periodic grating structures [24]. In this method, the electromagnetic field is expressed as homogenous in the direction of wave propagation ($+z$-direction in our model) and periodic in either or both of the x-and y-direction, according to Maxwell's equations in Fourier space. After expanding fields in each layer, we then applied proper boundary conditions to find the unknown field amplitude coefficients. For our purposes, we considered the permittivity of the metal layer, $\varepsilon(x, y)$, as periodic in both the x- and y-direction with the periodic wave vector components in those directions of the layer expressed as

$$k_{x,mn} = k_x + 2\pi m/L_x \tag{1}$$

$$k_{y,mn} = k_y + 2\pi n/L_y \tag{2}$$

where m, n are integers representing diffraction orders from $-N/2$ to $+N/2$ (N is the number of harmonics used to expand the fields inside the layer); k_x and k_y represent the x- and y-direction wave vector components for incident media; and L_x, L_y are unit cell periodicity in x- and y-direction, respectively. We expanded the permittivity distribution of the metallic layer following the formula outlined by Li [25, 26]. After expanding the permittivity for an inhomogeneous layer, a matrix representation of internal fields in that layer is possible if we write Maxwell's curl equations in the partial differential form.

$$\frac{\partial}{\partial z}\begin{bmatrix} E_x \\ E_y \end{bmatrix} = k_0 P \begin{bmatrix} H_x \\ H_y \end{bmatrix} \tag{3}$$

$$\frac{\partial}{\partial z}\begin{bmatrix} H_x \\ H_y \end{bmatrix} = k_0 Q \begin{bmatrix} E_x \\ E_y \end{bmatrix} \tag{4}$$

where P, Q are matrices computed from the vector components and permittivity expansion, clearly outlined by [27]. Using Eq. (3) and Eq. (4), a matrix wave equation can be written and solved by finding the eigenvalues and eigenvectors of matrix Φ^2 mentioned in Eq. (6).

$$\frac{\partial^2}{\partial z^2}\begin{bmatrix} E_x \\ E_y \end{bmatrix} - \Phi^2 \begin{bmatrix} E_x \\ E_y \end{bmatrix} = \begin{bmatrix} 0 \\ 0 \end{bmatrix} \tag{5}$$

$$\Phi^2 = PQ \tag{6}$$

The eigenvalues represent the propagation constants for the field harmonics, and the eigenvector represents the harmonic field orientation within the layer. The field solutions can then be written in matrix from as

$$\Theta(z) = \begin{bmatrix} E_x \\ E_y \\ H_x \\ H_y \end{bmatrix} = \begin{bmatrix} U & U \\ V & V \end{bmatrix} \begin{bmatrix} \exp(-\gamma z) & 0 \\ 0 & \exp(\gamma z) \end{bmatrix} \begin{bmatrix} A^+ \\ A^- \end{bmatrix} \tag{7}$$

$$V = QU\gamma^{-1} \tag{8}$$

In Eq. (7) and Eq. (8), U and V describe the eigenmodes of the electric fields and magnetic fields, respectively. γ represents the root square of the eigenvalue, and A^+, A^- represent the field amplitude coefficients for forward and backward propagating waves, respectively. There is no need to solve the eigenvalue problem of the homogeneous layer because there is no permittivity variation for the layer. Thus, its eigenvector matrix is an identity matrix, with eigenvalues that are simply the z components of the wavevectors computed from permittivity and other directional wavevector components. Finally, to solve boundary conditions, several approaches are available, and we followed the procedure outlined in [28].

2.2. Simulation Model

The proposed design of the metallic wire-based polarizer is shown in Fig. 1. We used gold as the metal and BK7 glass as a substrate. A single periodic cell is 170 nm (L_x) by 370 nm (L_y). L_x and L_y represents x and y directional period respecively. The depth, d, of the metal layer is 400 nm. Each small metal wire oriented along y-axis (termed as l_y) is 120 nm by 10 nm, respectively in length and width, and the air gap between successive small metal wires (l_{gx}) is 50 nm. The long metal wire oriented along the full length of x-axis (l_x) is 10 nm wide 170 nm in length, and the distance between this and each metal wire on both side (l_{gy}) is 60 nm. Our simulation model treats the light source as a monochromatic plane wave perpendicularly incident on the polarizer. For refractive index values, we used the data for Au from [29] and Schott AG datasheet for BK7 glass.

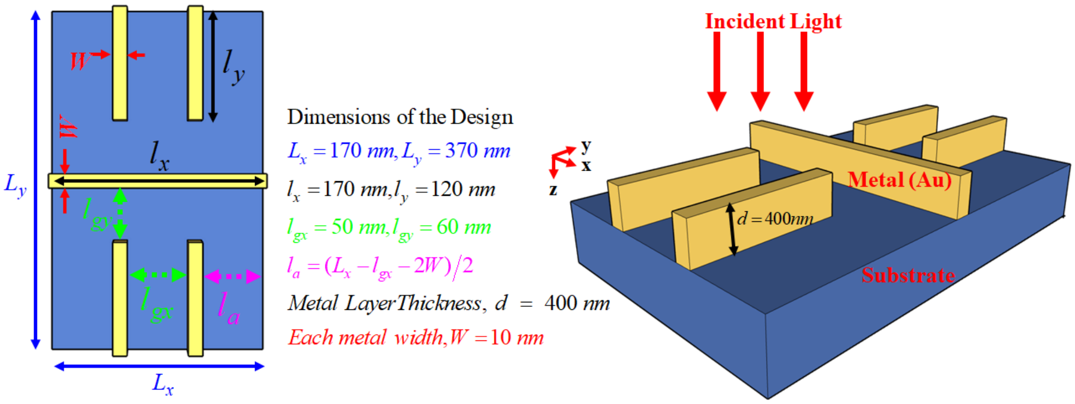

(a) (b)

Figure 1. Unit cell of the proposed polarizer. (a) Top view with geometrical parameters. (b) 3D side view. Dimensions are mentioned in the figure.

3. RESULTS AND DISCUSSION

Figure 2 presents the transmittance, reflectance, and absorption characteristics of our proposed polarizer. We simulated the device in the wavelength range from 400 to 1900 nm. The polarizer passes x-polarization in most of the visible band with more than 80% transmittance while y-polarization transmittance stays roughly at or below 10%. In the near-infrared region (from about 1300 to 1900 nm), y-polarization is passed by the polarizer with more than 80% transmittance and that same value is below 15% for x-polarization. The performance continues till $\sim 30^\circ$ for the incident angle and then drops and limits dual-band performance.

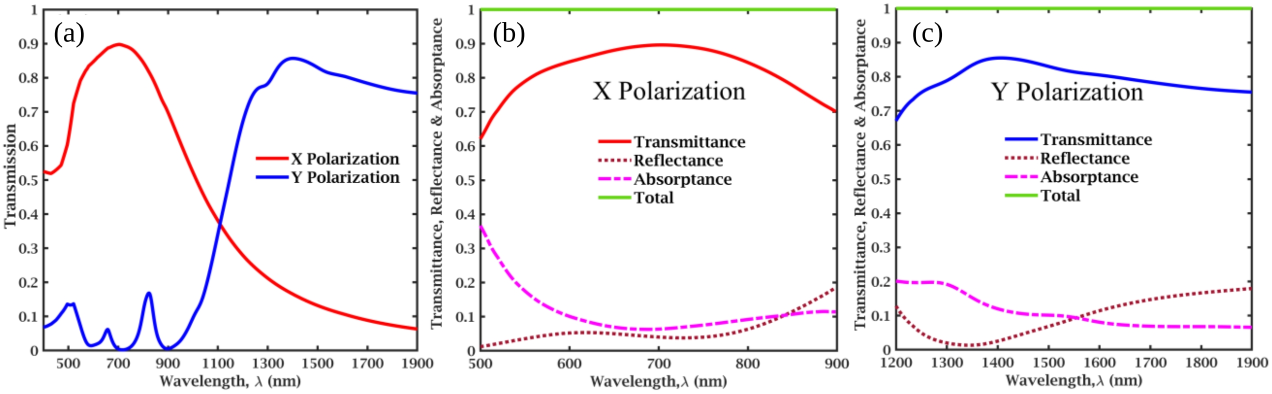

Figure 2. Transmittance, reflectance, and absorption characteristics. (a) Transmission for x- and y-polarization in the 400 to 1900 nm region. Transmittance, reflectance, and absorption characteristics for (b) x-polarization in the visible region, (c) y-polarization in the near infrared region.

To understand the full operational behavior of the proposed polarizer, it is necessary to examine the overall transmittance, reflectance and absorptance behavior of each polarization under varying parameters. The plots in Fig. 3 reflect these aspects of the polarizer, and Fig. 3(a) shows the transmission, reflection and absorption characteristics of x-polarization over the full wavelength range of our simulation. The designed structure enables two different types of air gaps, or slits, to form in the unit cell. Along the x-direction, the four small vertical metal wires create air gaps (l_{gx}) among successive

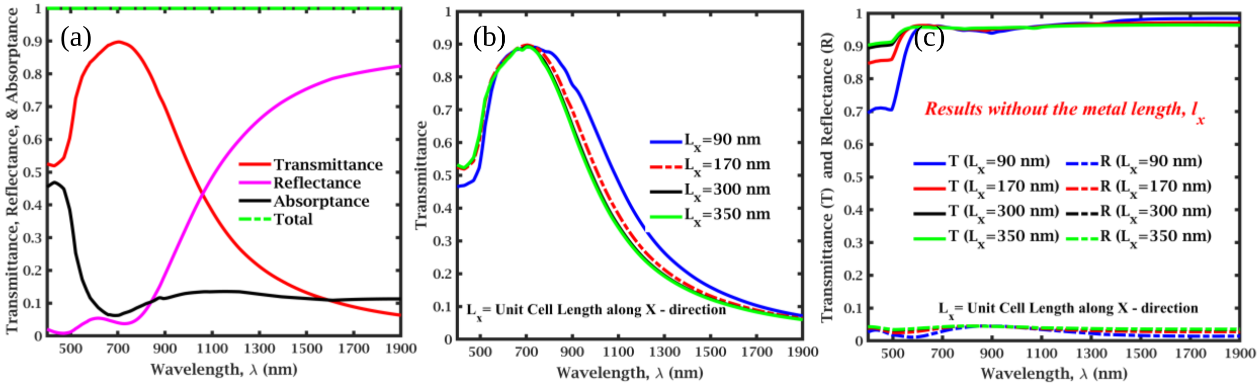

Figure 3. Transmittance, reflectance, and absorption characteristics for x-polarization with normal incidence of light (a) in the 400 to 1900 nm region, (b) transmittance different x-direction period lengths (L_x) with a constant air gap in the x-direction ($l_{gx} = 50\,\text{nm}$), and (c) transmittance and reflectance curves without the long metal wire (l_x) at a constant x-direction period ($L_x = 170\,\text{nm}$) and air gap ($l_{gx} = 50\,\text{nm}$).

wires, whereas in the y-direction, air gaps or slits (l_{gy}) are produced by the long horizontal metal wire (l_x) and the small vertical metal wires (l_y) on both sides of the long metal wire. We designed the unit cell so the structure offers different slits for differently polarized light, and we can control the polarization behavior in different wavelength ranges by appropriate choice of metal length and widths. These slits enable strong light confinement through Fabry-Perot resonance (i.e., slit resonance). This well-known phenomenon explains the high broadened transmission for x-polarization at lower frequencies that, with a decreased period and decoupled slit and grating resonances (i.e., the constructive interference of scattered light by a periodic grating), broadens the transmission peak [30]. According to Wang et al., typical wire grid polarizers working in the visible range have a period of less than 150 nm [31]. This length and the metal wire position are vital because they define the slit length, which in turn changes the resonant cavity length and controls the spectral position of the transmission peak. With a longer slit, the transmission peak will move into the infrared region. In this paper, our unit cell is 170 nm in the x-direction (L_x, also known as the periodicity in the x-direction).

To further illustrate this point, we simulated the design by reducing the period in the x-direction and keeping the air gap constant between the metallic wire in the x-direction. The result in Fig. 3(b) resembles existing theory with the broadest transmittance curve produced for the lowest x-directional period. By decreasing the period, the grating resonance is gradually pushed away from the slit resonance at shorter wavelengths and the resonances decouple. In response, the slit resonance acts to broaden the transmission peak, and transmission dips at the lowest wavelengths in our range. To create a polarizer that behaves differently in two different wavelength ranges, we introduced a long metal wire (l_x) along x-axis with an air gap on both sides of it. As clear from Fig. 3(c), our polarizer behaves as an ultra-broadband x-polarizer without the long metal wire which, when present, acts to prevent the slit resonance from dominating over the full simulation wavelength range. The high reflectance value at longer wavelengths in Fig. 3(b) is due to the large impedance mismatch at the metal-air interface in the presence of the long metal wire (l_x), causing slit resonance and transmittance to diminish.

Figure 4 displays the electric field intensity ($|E|^2$) spatial distribution for x-polarization at different wavelengths. At 700 and 1400 nm, we observe peaks for the x-and y-polarization, respectively, and around 1100 nm, the polarization transmittance curves cross each other i.e., they show same numerical value. A well confined electric field is present between air gaps due to the dominance of slit resonance at 700 nm in Fig. 4(a). As wavelength increases, electric field intensity begins to decrease inside the slits due to the aforementioned impedance mismatch at the metal-air interface caused by the long metal wire (l_x). This trend is evident in Fig. 4(b) and Fig. 4(c).

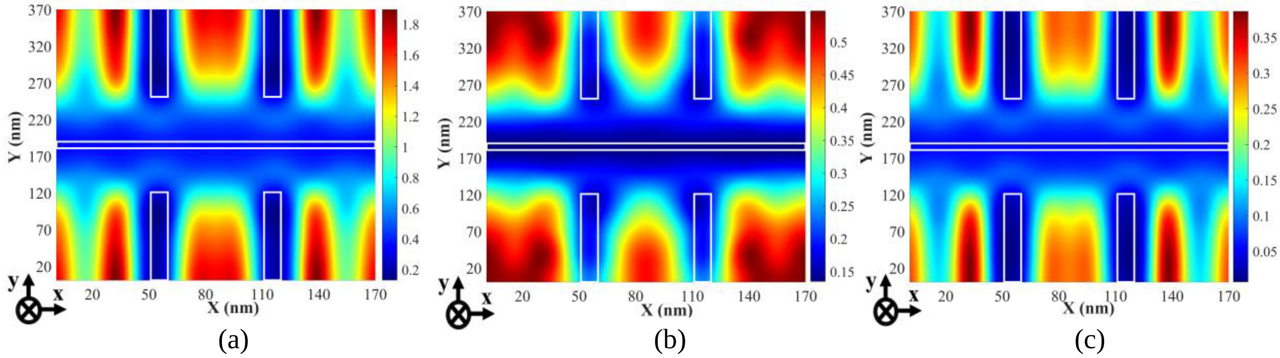

(a) (b) (c)

Figure 4. Electric field intensity ($|E|^2$) spatial distribution at the middle of metal layer ($d = 200$ nm) for x-polarization at (a) 700 nm, (b) 1100 nm, and (c) 1400 nm. Metal wires are indicated by white solid lines.

We plotted the transmittance, reflectance, and absorptance for y-polarized normal incident light and varied certain parameters to explore the working principle of our polarizer. The nearly identical nature of Fig. 5(a) and Fig. 5(b) demonstrate the negligible effect of the long metal wire (l_x) on y-polarization characteristics since that metal wire is perpendicular to the y-polarized field. Next, we simulate y-polarization behavior keeping the period in y-direction constant and reducing the length of

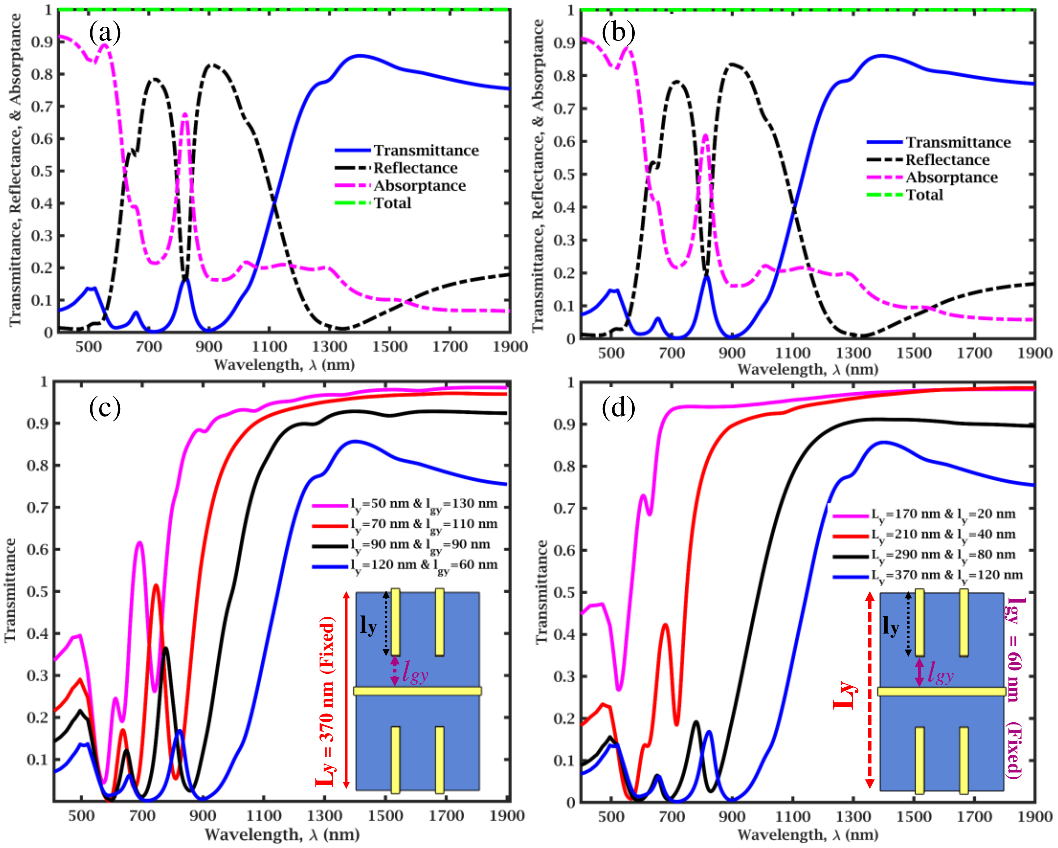

Figure 5. Transmittance, reflectance, and absorption characteristics for y-polarization with normal incidence of light in the 400 to 1900 nm region (a) with the long metal wire (l_x), (b) without the long metal wire (l_x), (c) at constant y-direction period ($L_y = 370$) with varying small wire's metal length (l_y) and, consequently, varying y-direction air gap (l_{gy}), and (d) at constant y-direction air gap ($l_{gy} = 60\,\text{nm}$) with varying y-direction period (L_y) and, consequently, varying small metal wire's length (l_y).

small metal wires (l_y). From results in Fig. 5(c), we deduce that the air-gap-to-period ratio controls the transmittance characteristics. The highest ratio of the air gap to period (pink curve in Fig. 5(c) where $l_{gy}/L_y = 130/370 = 0.35$) provides the broadest transmittance curve for y-polarization. The same concept is true for x-polarization too. In Fig. 3(b), the broadest transmission is achieved at the highest ratio of the air gap to period ($l_{gx}/L_x = 50/90 = 0.56$, blue curve). Additionally, at the highest air-gap-to-period ratio, the transmittance curve extends over a greater range of wavelengths, including lower values. To validate this idea, we varied the period in the y-direction at a constant air gap (60 nm). The result of this simulation is shown in Fig. 5(d), and we obtain similar results to those depicted in Fig. 5(c). Again, we find the highest ratio of air-gap-to-period produces the most broadened transmittance curve and covers a greater range of wavelengths. From Figs. 5(c) & 5(d), we can conclude that by keeping a constant air-gap-to-period ratio, similar performances can be obtained by either increasing the air gap or reducing the period.

The electric field intensity plots shown in Fig. 6 reveal the strong confinement of light in the air gap, clearly validating the idea that strong slit resonance at the highest air-gap-to-period ratio controls the transmittance of y-polarization.

The dependency of transmission characteristics on the air-gap-to-period ratio of our proposed metallic plasmonic polarizer is a geometric effect due to constructive interference of propagating waveguide modes within the slit. Lindberg et al. delineated a behavior of this nature in a metallic film with a subwavelength slit [32]. According to their work, the transmission behavior of slit-based metallic structures weakly depends on the dielectric constant of the metal, which explains their similar

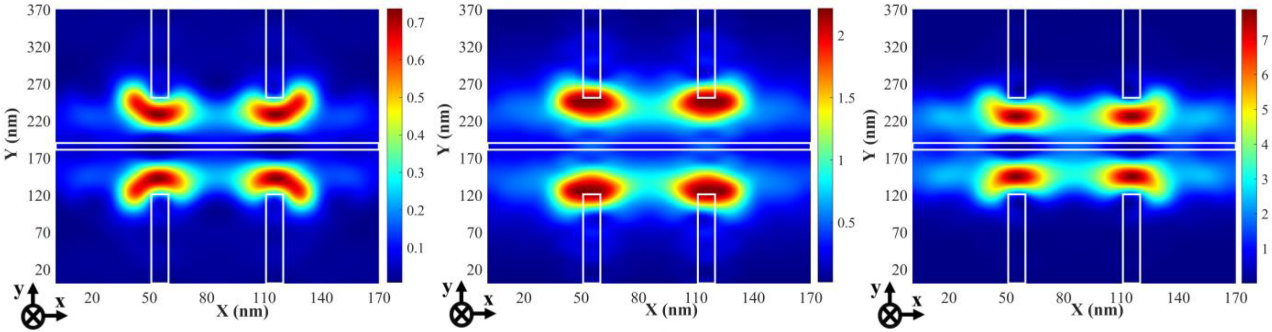

(a) (b) (c)

Figure 6. Electric field intensity ($|E|^2$) spatial distribution at the middle of metal layer ($d = 200\,\text{nm}$) for y-polarization at (a) 700 nm, (b) 1100 nm, and (c) 1400 nm. Metal wires are indicated by white solid lines.

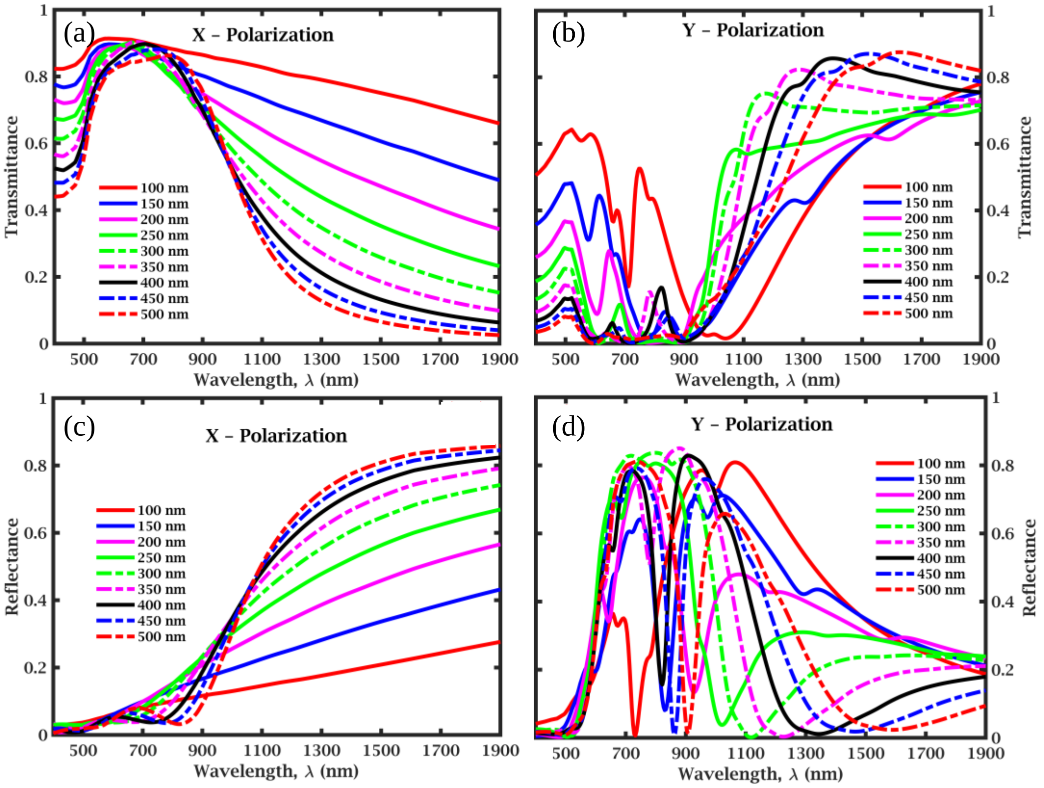

Figure 7. Effects of metal layer thickness on (a) transmittance of x-polarization, (b) transmittance of y-polarization, (c) reflectance of x-polarization, and (d) reflectance of y-polarization. Legends in each graph represents metal layer thickness.

results for Ag, Al, and Au. By increasing the width of the slit, the transmission peak can be broadened because a wider air gap enables more modes to propagate within the slits, thereby increasing the overall transmission.

Figure 7 depicts the effects of metal layer thickness on the transmission and reflection of the polarizer. As visible in Figs. 7(a) & 7(c), increasing the metal thickness results in decreased transmission and increased reflection of x-polarized light. Since we used a long metal wire (l_x) parallel to the incident electric field for x-polarization, increasing metal thickness increases its resistivity which limits electric field penetration of the metal layer, thereby decreasing transmission and increasing reflection. Our previous result in Fig. 3(c) also validates this resistive effect of metal for x-polarization in our design, where the absence of the long metal wire provides higher transmission and lower reflection for the entire operating wavelength range. For y-polarization, an increment of the metal layer thickness shifts the transmission peak at the longer wavelength with increased value.

With increased metal layer thickness, for y-polarization, the air hole depth increases leading to an electric field enhancement in those air gaps (l_{gy}). Conversely, the long metal wire which is parallel to the incident electric field has limited effects. The impact of the increased air gap for y-polarization is also evident in Fig. 5(c), where the most broadened transmission curve for y-polarization coincides with the greatest air gap value.

Continuing the discussion of the impact of metal in our design, we changed the width of the metallic wires and plotted the results in Fig. 8. We used four small metal wires (l_y) and one long metal wire (l_x), so for Fig. 8, while changing the width of one type, keeping the other type constant, i.e., keeping the width of l_x fixed when we change the width of l_y. Changing the metal wire's width is analogous to changing the design's air gap. Increasing the width of long metal l_x, which lies along the x-axis, affects x-polarization by increasing the reflection and narrowing the transmission with reduced peak value [Fig. 8(a)]. For y-polarization, the effect is negligible and shows similar results in reflection and transmission for all width values for l_x [Fig. 8(b)]. Increasing the width of l_x acts as a resistivity increment for x-polarized light while reducing the air gap for y-polarized light. On the other hand, increasing the width of l_y reduces air gap for x-polarization and increases of air gap for y-polarization. Therefore, the transmission reduces for x-polarization [Fig. 8(c)] and vice versa for y-polarization [Fig. 8(d)]. Additionally, based on our simulation results of transmitted electric and magnetic fields, we see low surface impedance for both polarizations in their specific passband. For y-polarization, the proposed structure shows lower impedance than it is for x-polarization because of the placement of the metal wires, as discussed above in the paper.

Finally, we analyze the performance of the proposed design based on two well-known metrics for polarizer: the degree of polarization and the polarization extinction ration (PER; also known as the

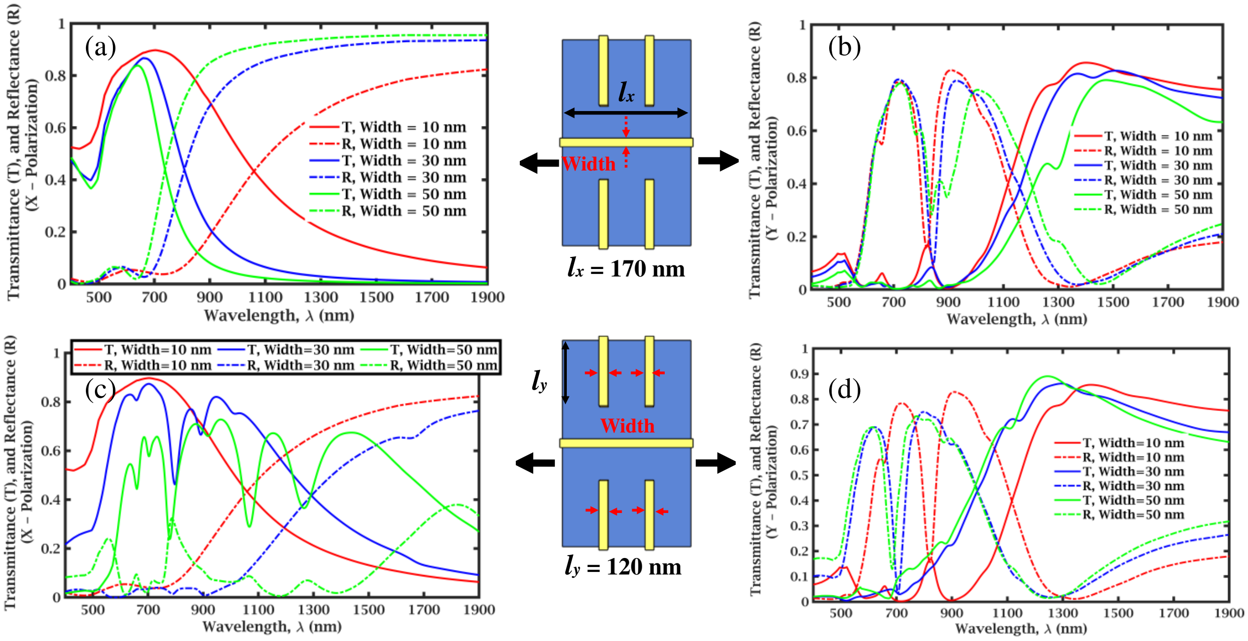

Figure 8. Effects of metal width on transmittance for (a) x-polarization, (b) y-polarization. Effects of metal width on reflectance for (c) x-polarization, and (d) y-polarization. Corresponding variable metal width is indicated in the design.

extinction ratio, or ER). Degree of polarization is defined as

$$Degree\ of\ Polarization = \left|\frac{T_1 - T_2}{T_1 + T_2}\right|. \tag{9}$$

where T_1 represents the transmission due to the incident light perpendicular to the polarizer axis, and T_2 represents the transmission due to the incident light parallel to the polarizer axis. For our analysis, T_1 represents the transmission for x-polarization and T_2 represents the transmission for y-polarization in the wavelength range of 400 to 1100 nm, and vice versa in the 1100 to 1900 nm region. The vertical dotted black line in Fig. 9 indicates the separation of x & y polarization passing regions. The proposed design behaves excellently with a degree of polarization close to or greater than 80% (0.8) in the specified range with the desired polarization. The other performance metric, polarization extinction ratio (PER) is a measure of the degree to which light is confined in a principal linear polarization mode, defined as

$$PER = 10\left|\log\frac{P_{principle}}{P_{orthogonal}}\right| (\text{dB}) \tag{10}$$

In the 400–1100 nm range, the principal polarization for our design is x, and orthogonal polarization is y. For, 1100–1900 nm, the principal polarization is y, and orthogonal polarization is x. For the proposed device, the solid blue line in Fig. 9 shows a PER in the spectral regions of interest.

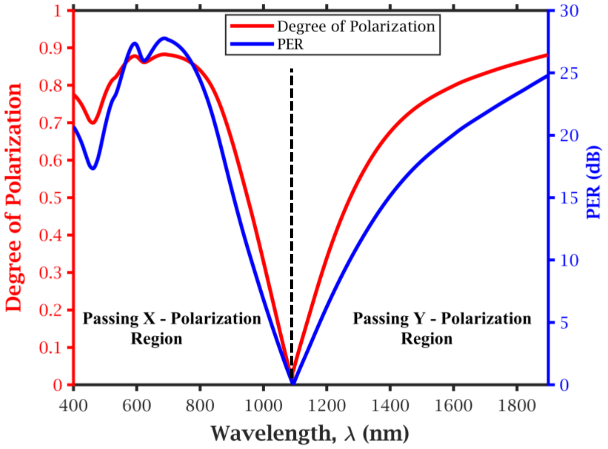

Figure 9. Degree of polarization and polarization extinction performance of the proposed polarizer.

Continuing this research, we aim to improve the design to operate for circular polarization states, creating multiple small bands with specific polarization to pass/absorb/reflect and finally to apply in nonlinear scenarios.

4. CONCLUSION

We designed a plasmonic Au multi-scaled wire-based nanostructured polarizer that allows two different polarizations to pass in two different bandwidths. We judiciously positioned a long metal wire along the x-direction and tuned the polarizer characteristics to achieve the desired broad transmission at two different bands for perpendicular polarizations. The bandwidth of transmission can be tuned by appropriate selection of metal wire length and by inducing strong, localized slit resonance. Achieving a polarizer that we have shown in our paper might direct researchers to dig more in the areas like in nonlinear optics, as an integrated polarization-sensitive dichroic filter, to discriminate the fields emitted in a 3-wave mixing process (such as sum or difference frequency generation), in fluorescence and in nonlinear imaging, to separate sample's emission both in terms of wavelength and polarization, in integrated photonics, where you cannot fit a bulky dichroic filter.

ACKNOWLEDGMENT

A.S. acknowledges the support of the Air Force Office of Scientific Research (AFOSR) through the grant FA9550-20-1-0046.

DISCLOSURES

The authors declare no conflicts of interest.

REFERENCES

1. Qin, F., L. Ding, L. Zhang, F. Monticone, C. C. Chum, J. Deng, S. Mei, Y. Li, J. Teng, M. Hong, S. Zhang, A. Alù, and C.-W. Qiu, "Hybrid bilayer plasmonic metasurface efficiently manipulates visible light," *Sci. Adv.*, Vol. 2, e1501168, 2016.
2. Astilean, S., Ph. Lalanne, and M. Palamaru, "Light transmission through metallic channels much smaller than the wavelength," *Optics Communications*, Vol. 175, 265–273, 2000.
3. Zhang, D., P. Wang, X. Jiao, et al., "Polarization properties of subwavelength metallic gratings in visible light band," *Appl. Phys. B*, Vol. 85, 139–143, 2006.
4. Frese, D., Q. Wei, Y. Wang, L. Huang, and T. Zentgraf, "Nonreciprocal asymmetric polarization encryption by layered plasmonic metasurfaces," *Nano Lett.*, Vol. 19, 3976–3980, 2019.
5. Hsiao, H.-H., C. H. Chu, and D. P. Tsai, "Fundamentals and applications of metasurfaces," *Small Methods*, Vol. 1, 1600064, 2017.
6. Mizner, N., W. L. Barnes, and I. R. Hooper, "Plasmonic meta-atoms and metasurfaces," *Nature Photonics*, Vol. 8, 889–898, 2014.
7. Bai, B., L. Liu, R. Chen, and Z. Zhou, "Low loss, compact TM-pass polarizer based on hybrid plasmonic grating," *IEEE Photonics Technology Letters*, Vol. 29, 607–610, 2017.
8. Wang, B., S. Blaize, and R. Salas-Montiel, "Nanoscale plasmonic TM-pass polarizer integrated on silicon photonics," *Nanoscale*, Vol. 11, 20685–20692, 2019.
9. Huang, Z., H. Park, E. P. J. Parrott, H. P. Chan, and E. Pickwell-MacPherson, "Robust thin-film wire-grid thz polarizer fabricated via a low-cost approach," *IEEE Photonics Technology Letters*, Vol. 25, 81–84, 2013.
10. Huang, Z., E. P. J. Parrott, H. Park, H. P. Chan, and E. Pickwell-MacPherson, "High extinction ratio and low transmission loss thin-film terahertz polarizer with a tunable bilayer metal wire-grid structure," *Opt. Lett.*, Vol. 39, 793–796, 2014.
11. Ding, F., Z. Wang, S. He, V. M. Shalaev, and A. V. Kildishev, "Broadband high-efficiency half-waveplate: A supercell-based plasmonic metasurface approach," *ACS Nano*, Vol. 9, 4111–4119, 2015.
12. Huang, C.-P., Y.-L. Wang, and Y. Zhang, "Interference-type plasmonic polarizers and generalized law of Malus," *J. Opt.*, Vol. 21, 105001, 2019.
13. Xia, J., Z. Yuan, C. Wang, C. He, J. Guo, and C. Wang, "Design and fabrication of a linear polarizer in the 8–12 μm infrared region with multilayer nanogratings," *OSA Continuum*, Vol. 2, 1683–1692, 2019.
14. Pelzman, C. and S.-Y. Cho, "Polarization-selective optical transmission through a plasmonic metasurface," *Appl. Phys. Lett.*, Vol. 106, 251101, 2015.
15. Han, C. and W. Y. Tam, "Plasmonic ultra-broadband polarizers based on Ag nano wire-slit arrays," *Appl. Phys. Lett.*, Vol. 106, 081102, 2015.
16. Tang, S., F. Ding, T. Jiang, T. Cai, and H.-X. Xu, "Polarization-selective dual-wavelength gap-surface plasmon metasurfaces," *Opt. Express*, Vol. 26, 23760–23769, 2018.
17. Li, X., S. Tang, F. Ding, et al., "Switchable multifunctional terahertz metasurfaces employing vanadium dioxide," *Sci, Rep.*, Vol. 9, 5454, 2019.

18. Qiu, X., J. Shi, Y. Li, and F. Zhang, "All-dielectric multifunctional transmittance tunable metasurfaces based on guided mode resonance and ENZ effect," *Nanotechnology*, Vol. 32, 065202, 2021.
19. Cui, J., Q. F. Nie, Y. Ruan, S. S. Luo, F. J. Ye, and L. Chen, "Dual-polarization wave-front manipulation with high-efficiency metasurface," *AIP Advances*, Vol. 10, 095003, 2020.
20. Deshpande, R. A., F. Ding, and S. Bozhevolnyi, "Dual-band metasurfaces using multiple gap-surface plasmon resonances," *ACS Appl. Mater. Interfaces*, Vol. 12, 1250–1256, 2020.
21. Ebbesen, T., H. Lezec, H. Ghaemi, et al., "Extraordinary optical transmission through sub-wavelength hole arrays," *Nature*, Vol. 391, 667–669, 1998.
22. Lochbihler, H., "Surface polaritons on gold-wire gratings," *Phys. Rev. B*, Vol. 50, 4795–4801, 1994.
23. Astilean, S., Ph. Lalanne, and M. Palamaru, "Light transmission through metallic channels much smaller than the wavelength," *Optics Communications*, Vol. 175, 265–273, 2000.
24. Moharam, M. G. and T. K. Gaylord, "Rigorous coupled-wave analysis of planar-grating diffraction," *J. Opt. Soc. Am.* Vol. 71, 811–818, 1981.
25. Li, L., "Use of Fourier series in the analysis of discontinuous periodic structures," *J. Opt. Soc. Am. A*, Vol. 13, 1870–1876, 1996.
26. Li, L., "New formulation of the Fourier modal method for crossed surface-relief gratings," *J. Opt. Soc. Am. A*, Vol. 14, 2758–2767, 1997.
27. Moharam, M. G., E. B. Grann, D. A. Pommet, and T. K. Gaylord, "Formulation for stable and efficient implementation of the rigorous coupled-wave analysis of binary gratings," *J. Opt. Soc. Am. A*, Vol. 12, 1068–1076, 1995.
28. Moharam, M. G. and T. K. Gaylord, "Diffraction analysis of dielectric surface-relief gratings," *J. Opt. Soc. Am.*, Vol. 72, 1385–1392, 1982.
29. Johnson, P. B. and R. W. Christy, "Optical constants of the noble metals," *Phys. Rev. B*, Vol. 6, 4370–4379, 1972.
30. Zhou, J. and L. Guo, "Transition from a spectrum filter to a polarizer in a metallic nano-slit array," *Sci. Rep.*, Vol. 4, 3614, 2014.
31. Wang, J. J., F. Walters, X. Liu, P. Sciortino, and X. Deng, "High-performance, large area, deep ultraviolet to infrared polarizers based on 40 nm line/78 nm space nanowire grids," *Appl. Phys. Lett.*, Vol. 90, 061104, 2007.
32. Lindberg, J., K. Lindfors, T. Setälä, M. Kaivola, and A. T. Friberg, "Spectral analysis of resonant transmission of light through a single sub-wavelength slit," *Opt. Express*, Vol. 12, 623–632, 2004.